

Uncertainty in phosphine photochemistry in the Venus atmosphere prevents a firm biosignature attribution

Fabian Wunderlich¹, John Lee Grenfell¹, and Heike Rauer^{1,2,3}

¹ Institut für Planetenforschung, Deutsches Zentrum für Luft- und Raumfahrt, Rutherfordstraße 2, 12489 Berlin, Germany
e-mail: wunderlich.fabian@googlegmail.com

² Zentrum für Astronomie und Astrophysik, Technische Universität Berlin, Hardenbergstraße 36, 10623 Berlin, Germany

³ Institut für Geologische Wissenschaften, Freie Universität Berlin, Malteserstr. 74-100, 12249 Berlin, Germany

Received 29 October 2021 / Accepted 28 March 2023

ABSTRACT

Context. The possible detection of phosphine (PH₃) in the clouds of Venus has raised the question as to which processes could produce such large abundances of PH₃. Previous studies suggested that abiotic processes including photochemical production cannot explain the claimed PH₃ concentrations. However, the photochemistry of phosphorus-bearing species in the atmosphere of Venus is not well known.

Aims. We aim to assess the abiotic production of PH₃ considering the effect of uncertainties in the chemical rate coefficients of phosphorus-containing reactions.

Methods. Using a photochemical column model, we simulated Venus-like conditions and varied the chemical rate coefficients with a Monte Carlo (MC) approach in order to estimate the associated error in the PH₃ abundances throughout the atmosphere.

Results. Current uncertainties and missing data in photochemical rate coefficients lead to a variation of about six orders of magnitude in the modelled PH₃ abundance on Venus, assuming photochemical production of PH₃ from tetraphosphorus hexoxide (P₄O₆) pathways. Our results suggest an abiotically produced upper limit of 2 ppb PH₃ between 50 and 60 km. These concentrations are in the range of a recent reanalysis of Atacama Large Millimeter Array (ALMA) data, suggesting planet-averaged abundances in PH₃ of 1–4 ppb above 55 km. Future observations of phosphorus monoxide (PO) on Venus would be beneficial for increasing our confidence in assessing PH₃ as a biosignature.

Conclusions. We conclude that due to the large uncertainties in phosphorus chemistry, even a firm detection of several ppb PH₃ in the Venus atmosphere would not necessarily mean a biological origin.

Key words. planets and satellites: atmospheres – astrobiology – astrochemistry – planets and satellites: terrestrial planets

1. Introduction

The recent claimed detection of 20±10 ppbv of phosphine (PH₃) in the cloud decks of Venus (Greaves et al. 2021a) based on disk-averaged observations at millimeter wavelengths has generated considerable discussion. Snellen et al. (2020) repeated the data analysis of Greaves et al. (2021a) and suggested a detection significance of only 2σ, which implied that instruments with a higher sensitivity are required. Thompson (2021) performed a bootstrapping analysis on the Greaves data, but was not able to recover a statistically significant signal for 20 ppbv PH₃. Villanueva et al. (2021) and Lincowski et al. (2021) argued that the claimed PH₃ signal could be reproduced by assuming plausible mesospheric SO₂ abundances of around 10 ppbv or more. Akins et al. (2021) suggested, however, that the previously assumed 10 ppbv SO₂ limit is unlikely to be detected by Atacama Large Millimeter Array (ALMA) data. Encrenaz et al. (2020) suggested that an upper limit of 5 ppbv PH₃ is significant at the 3σ level based on disk-averaged observations at 10.5 μm. Trompet et al. (2021) suggested an upper limit of 0.4 ppb at 61 km for high latitudes and an upper limit of 6–8 ppb for equatorial regions. Greaves et al. (2020) recovered the PH₃ signal in the Venus atmosphere with 5σ confidence and suggested planet-averaged abundances of PH₃ of 1–4 ppb between 55 and 60 km. Most recently, Greaves et al. (2021b) concluded that the net abundances of PH₃ are about 20 ppb from *James Clerk Maxwell*

Telescope (JCMT) data and 7 ppb from ALMA data. A recent re-analysis by Greaves et al. (2022) of their millimeter wavelength data suggested low levels (~10%) of SO₂ contamination in the PH₃ signal. In anoxic terrestrial atmospheres, PH₃ has been proposed as a potential biosignature (see Bains et al. 2019; Sousa-Silva et al. 2020). If the detection of PH₃ with concentrations in the ppb level in the Venusian clouds is real, then Greaves et al. (2021a) and Bains et al. (2021) conclude that such large abundances of PH₃ cannot be accounted for by currently known abiotic processes, suggesting a biological origin. Recently, Patel et al. (2022) showed that in the Venus clouds, a potential thermal and radiation habitable zone would extend from 59 to 48 km.

Possible abiotic source of PH₃ have been investigated by various works. McTaggart (2022) simulated cosmogenic production of phosphorus in the atmosphere of Venus, but concluded that the amount of phosphorus produced is insufficient to explain the proposed concentrations of PH₃. Truong & Lunine (2021) suggested that volcanic phosphides ejected into the clouds are a plausible abiotic source of the Venusian phosphine. However, Bains et al. (2022) argued that this mechanism requires an implausibly high eruption volume. Omran et al. (2021) proposed possible atmospheric abiotic pathways of PH₃ from meteoritic and geological sources. They concluded that the detection of phosphine alone is likely not to be a decisive indicator of life. The photochemistry of phosphorus-bearing species in these environments is not well known (see e.g. Bains et al. 2021).

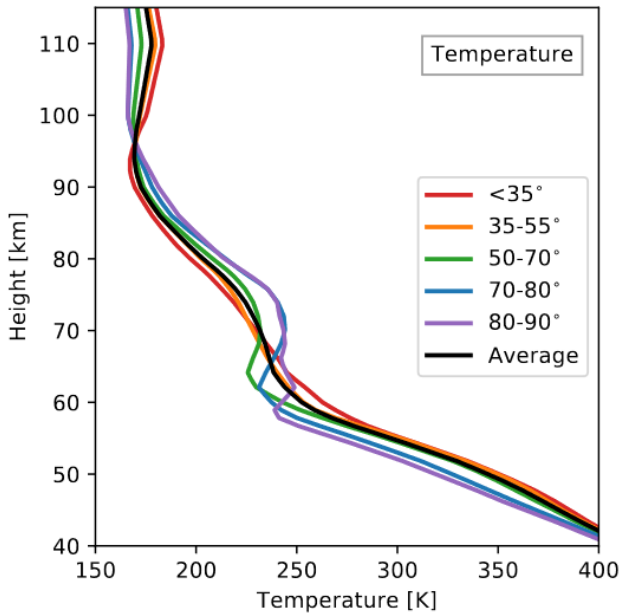


Fig. 1. Input temperature profiles of modern Venus for latitudes below 35° (red line), 35–55° (orange line), 50–70° (green line), 70–80° (blue line) and 80–90° (purple line) taken from Haus et al. (2013) and a global average (black line).

Greaves et al. (2021a) and Bains et al. (2021) applied a detailed chemical network and used analogous nitrogen species reaction kinetics for several phosphorus-bearing chemical reactions with unknown rate coefficients. They suggested an abiotic upper limit of about 0.2 parts per quadrillion (ppq) (2×10^{-16}) PH_3 around 50 km.

In this work, we reassess the maximum chemical production of PH_3 in the atmosphere of Venus by considering the uncertainties in its photochemical production pathways. Unlike previous works, we assume that phosphorus monoxide (PO) might be produced by destruction of tetraphosphorus hexoxide (P_4O_6), which was observed to be the main phosphorus-bearing gas on Venus with a mixing ratio of 2 ppmv below 25 km (see Krasnopolsky 1989). Section 2 describes the photochemical model and the scenarios. Section 3 shows results, and Sect. 4 provides some brief conclusions.

2. Method

2.1. Model description

1D-TERRA is a one-dimensional global mean, cloud-free, stationary atmospheric convection-photochemical-climate model capable of simulating a wide range of atmospheric temperatures (100–1000 K) and pressures (0.01 Pa– 10^3 bar) for different types of atmospheres such as those dominated by CO_2 , N_2 , H_2 , or H_2O (Scheucher et al. 2020; Wunderlich et al. 2020). In the present study, we use only the chemistry module BLACKWOLF and employ observed temperature profiles for modern Venus taken from Haus et al. (2013), as shown in Fig. 1. BLACKWOLF features a chemical network with over 1000 reactions for more than 100 species, including sulphur, chlorine, and phosphorus chemistry (Wunderlich et al. 2020, 2021). A detailed description of BLACKWOLF can be found in Wunderlich et al. (2020).

2.2. Phosphorus photochemical network

For the present work, we extended the phosphorus reaction network presented in Wunderlich et al. (2021) to 79 reactions A135, page 2 of 11

in total for 13 phosphorus-containing species. Our phosphorus photochemical network (PPN) was based on Greaves et al. (2021a) and Bains et al. (2021), but includes additional reactions such as the production of PO from PH and PH_2 . Appendix A shows the full list of PPN reactions, together with their rate coefficients and references. Reactions in Table A.1 marked with an asterisk indicate missing rate data and therefore use analogous rate coefficients in which phosphorus atoms present in reactant species are analogously replaced with nitrogen atoms for which rate data are available. Reactions for which the rate data are not available for temperatures below 750 K are indicated with a plus symbol in Table A.1. For all marked reactions, we calculated a log-normal uncertainty distribution as described in Appendix B.

2.3. Scenarios

We performed various scenarios simulating the atmosphere of modern Venus with our photochemistry module BLACKWOLF (see Table 1). For all scenarios, we used a fixed volume mixing ratio, f , at the surface for $f_{\text{N}_2} = 0.035$, $f_{\text{H}_2\text{O}} = 3 \times 10^{-5}$, $f_{\text{OCS}} = 4 \times 10^{-6}$, $f_{\text{CO}} = 2 \times 10^{-5}$, and $f_{\text{HCl}} = 5 \times 10^{-7}$, which provided model best fits to the observations. CO_2 was used as a fill gas to make up the remainder of the atmosphere. For scenarios 1b and 2b, SO_2 was fixed to 25 ppm at the surface, consistent with the VEGA 1 and VEGA 2 entry probes (Bertaux et al. 1996). For all other scenarios, SO_2 at the surface was set to 130 ppm, consistent with measurements above 30 km (see e.g. Bézard et al. 1993; Pollack et al. 1993; Marcq et al. 2008). To match the observed decrease in SO_2 mixing ratios above the clouds, we introduced an SO_2 sink of magnitude 7.1×10^{12} molecules $\text{cm}^{-2} \text{s}^{-1}$ in the cloud region in all scenarios except for scenarios 1b, 1c, 2b, and 2c.

In scenarios 1b and 2b, eddy diffusion coefficients were taken from Krasnopolsky (2007) below 47 km and from Krasnopolsky & Parshev (1981) above. All other scenarios used eddy diffusion coefficients below 47 km from Krasnopolsky (2012) and above 47 km from Krasnopolsky (2013). We used temperature profiles for modern Venus of five different latitudinal regions taken from Haus et al. (2013) and a weighted global mean temperature profile (see Fig. 1).

The phosphorus chemistry is introduced with the following three approaches. First, in scenarios 1a to 1h (termed “ PH_3 flux”), we used PH_3 input fluxes in the cloud layer between 50 and 60 km, similar to the scenario with directly produced PH_3 in the Venus clouds as performed by Greaves et al. (2020). All other phosphorus-containing species had zero input fluxes. Second, in scenarios 2a to 2h (termed “PO flux”), we used input fluxes of PO below 25 km. We assumed that PO is produced via P_4O_6 destruction. The other phosphorus-containing species had zero input fluxes. Third, in scenario 3 (termed “ H_3PO_4 flux”), we used H_3PO_4 input fluxes in the cloud layer between 50 and 60 km, similar to the abiotic scenario of Greaves et al. (2020). All other phosphorus-containing species had zero input fluxes.

The main motivation behind scenarios 2 and 3 was to test whether the observed concentrations of PH_3 could have arisen from atmospheric in situ chemical production via PO and H_3PO_4 , respectively. P_4O_6 is suggested to be the main phosphorus species at 25 km (Krasnopolsky 1989) and could be destroyed into PO and PO_2 via



In the lower atmosphere, the produced PO_2 can react with H and form more PO (Bains et al. 2021). For the conditions in the Venus

Table 1. Atmospheric scenarios for modern Venus.

Scenario	Phosphorus input	Surface SO ₂	SO ₂ removal	Eddy diffusion	Temperature profile
1a		130 ppm	Yes	K12 and K13	Average
1b		25 ppm	No	K81 and K07	Average
1c		130 ppm	No	K12 and K13	Average
1d	PH ₃ flux between 50 and 60 km	130 ppm	Yes	K12 and K13	Lat. <35°
1e		130 ppm	Yes	K12 and K13	Lat. 35–55°
1f		130 ppm	Yes	K12 and K13	Lat. 50–70°
1g		130 ppm	Yes	K12 and K13	Lat. 70–80°
1h		130 ppm	Yes	K12 and K13	Lat. 80–90°
2a		130 ppm	Yes	K12 and K13	Average
2b		25 ppm	No	K81 and K07	Average
2c		130 ppm	No	K12 and K13	Average
2d	PO flux below 25 km	130 ppm	Yes	K12 and K13	Lat. <35°
2e		130 ppm	Yes	K12 and K13	Lat. 35–55°
2f		130 ppm	Yes	K12 and K13	Lat. 50–70°
2g		130 ppm	Yes	K12 and K13	Lat. 70–80°
2h		130 ppm	Yes	K12 and K13	Lat. 80–90°
3	H ₃ PO ₄ flux between 50 and 60 km	130 ppm	Yes	K12 and K13	Average

Notes. The eddy diffusion profile “K12 and K13” uses the coefficients below 47 km from [Krasnopolsky \(2012\)](#) and above 47 km from [Krasnopolsky \(2013\)](#). For the “K81 and K07” eddy diffusion profile coefficients below 47 km are taken from [Krasnopolsky \(2007\)](#) and above 47 km from [Krasnopolsky & Parshev \(1981\)](#).

clouds, PO₂ might not be present in the gas-phase state (see e.g. [Haworth et al. 2002](#)). Due to the lack of rate coefficient data for P₄O₆, we cannot include the above reactions into our network. Instead, we assumed a range of input fluxes of PO in the lower atmosphere of Venus, where P₄O₆ is likely to be destroyed quickly ([Bains et al. 2021](#)).

2.4. MC simulations

We performed an MC analysis in which we randomly varied the coefficients of all reactions marked in the PPN (see Appendix A) within their log-normal uncertainty distribution (see Appendix B). We applied this technique to scenarios 1d–1h and 2d–2h with 200 MC runs for each scenario. Hence, the total number of MC runs of the PH₃ flux scenarios and PO flux scenarios was 1000 each. A test was performed in which the number of MC runs was doubled, but this did not lead to significant changes in the main outcome. We therefore conclude that 1000 runs lead to robust results.

3. Results

3.1. Model validation

We used our photochemical model for the first time to simulate the atmosphere of modern Venus from the surface up to about 120 km. To validate the model, we compare in Fig. 2 the results for scenarios 1a–1d, 1f and 1h (see details in Table 1) with the observational ranges for several key species.

In scenarios 1a and 1c the mixing ratios of SO₂ at the surface were fixed at 130 ppm, whereas in scenario 1b they are set to 25 ppm. For scenario 1a we added SO₂ removal in the cloud region to compensate for a missing SO₂ sink from cloud formation. Without this additional SO₂ sink (scenario 1c), the model predicts mixing ratios of SO₂ above 100 ppm from the surface up to 100 km. This leads to an overestimation of SO and OCS

compared to the observations above 60 km. An assumed low-surface SO₂ of 25 ppm leads to a decrease in SO₂ above the clouds at around 70 km. Scenario 1a with its enhanced removal rate, as discussed in the scenarios section, reproduces the observed SO₂ concentration profile; this suggests that the SO₂ decrease in the clouds cannot be explained by known photochemical processes alone (see also [Rimmer et al. 2021](#)).

Most scenarios in Fig. 2 overestimate the water abundances between 60 and 80 km. The simulation using the mid-latitude temperature profile (Scenario 1f) matches the observed H₂O concentrations in the middle atmosphere well. The concentrations of CO and HCl are less sensitive to both the choice of SO₂ at the surface and the temperature profile, and all scenarios agree with the observed concentration range. The model underestimates the decrease in carbonyl sulfide (OCS) in the clouds. The steep decline in observed OCS abundances by around two orders of magnitude from 30 to 40 km altitude is discussed in [Marcq et al. \(2018\)](#) and [Yung et al. \(2009\)](#). The high SO₂ scenarios with SO₂ removal fit the OCS observations best.

In order to test the impact of the OCS vertical behaviour, we performed an additional run. Here, starting with scenario 1a, we introduced an additional sink for OCS of 2.3×10^{12} molecules cm⁻² s⁻¹ in the clouds, as shown in Figure 3. The results suggest that with this sink, OCS (dashed blue line) matches the observed decrease with altitude between 30 km and 60 km well. PH₃ remained almost unaltered, whereas PO decreased quite considerably, suggesting that the production of PO from PH₃ is weakened.

3.2. Phosphorus fluxes

Figure 4 shows the concentration of PH₃ at 60 km with increasing input fluxes of PH₃, PO, and H₃PO₄. The observed global PH₃ abundances of 1–4 ppb at 60 km shown in [Greaves et al. \(2020\)](#) are reached with a PH₃ flux between 3×10^8 and 1×10^9 molecules cm⁻² s⁻¹. By comparison, on modern Earth, the

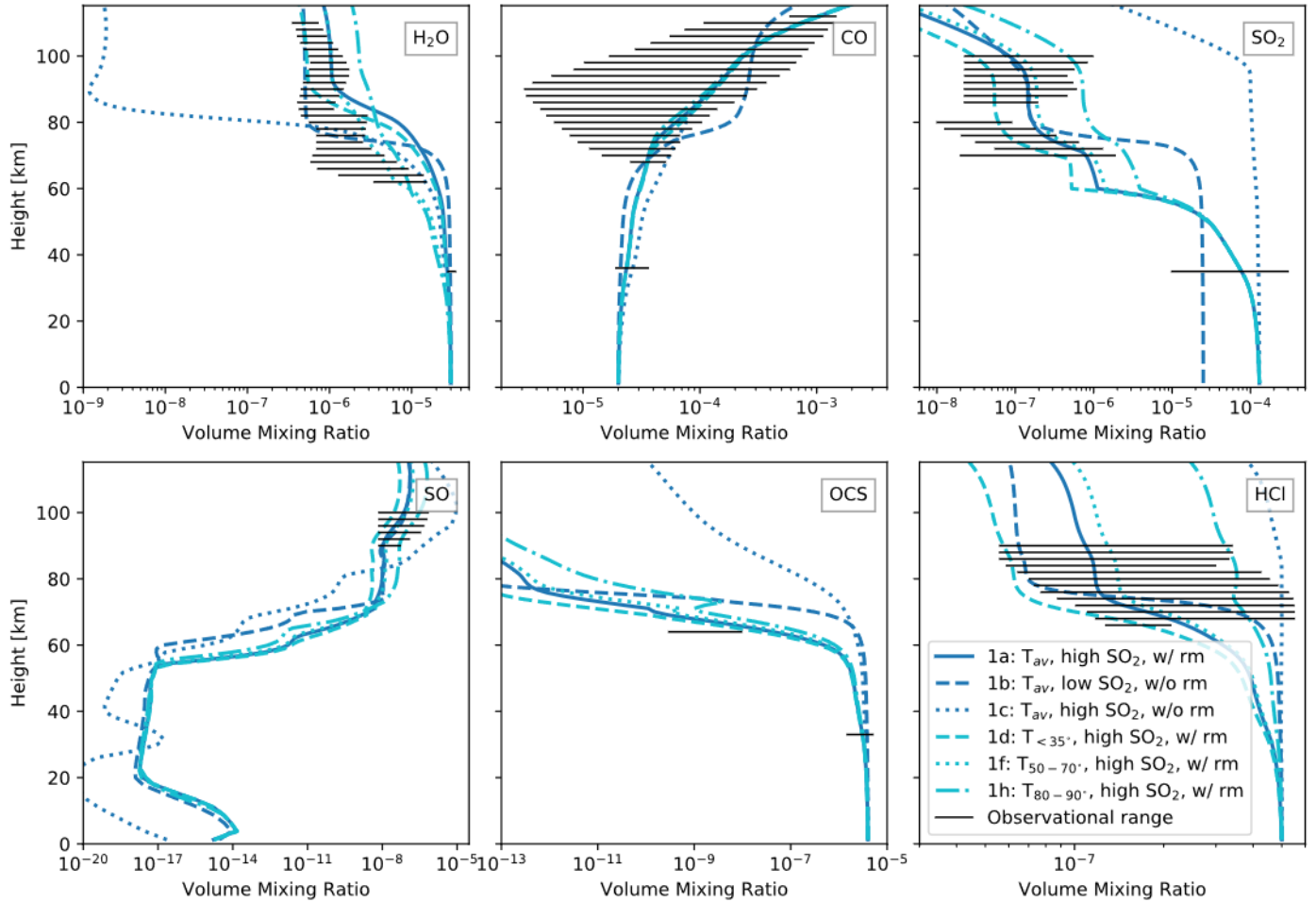


Fig. 2. Venus composition profiles for selected species predicted with our photochemistry model for scenarios 1a (solid blue line), 1b (dashed blue line), 1c (dotted blue line), 1d (dashed cyan line), 1f (dotted cyan line), and 1h (cyan dash-dotted line). For comparison, a range of observations is shown as solid, horizontal black lines. The observations of H_2O , CO , OCS , and SO_2 below the cloud top are taken from Svedhem et al. (2007) and Marcq et al. (2008). Observations of H_2O and CO above the clouds are taken from Bertaux et al. (2007) and Krasnopolsky (2012). The OCS observational range at 65 km is taken from Krasnopolsky (2010) and the range at 33 km from Marcq et al. (2008). For the observational range of SO_2 and SO above 60 km, we use data from Belyaev et al. (2012) and Sandor et al. (2010). Measurements of HCl above the cloud top are taken from Sandor & Clancy (2012) and Bertaux et al. (2007).

global PH_3 fluxes are not well determined, but are estimated to be around $4 \times 10^7 \text{ kg yr}^{-1}$ (Wang et al. (2022); $=4.4 \times 10^6 \text{ molecules cm}^{-2} \text{ s}^{-1}$). The production of PH_3 from formation pathways via PO reaches a maximum of 0.04 ppb PH_3 at 60 km for a PO flux of $1 \times 10^{10} \text{ molecules cm}^{-2} \text{ s}^{-1}$ below 25 km. A higher PO flux leads to an enhanced production of O_2 in and below the clouds and to weakened production of PH_3 via PO pathways in the clouds (see Fig. 5).

Large abundances of O_2 are not expected in the hot, reducing lower atmosphere of Venus, and early measurements by Oyama et al. (1979) that suggested around 43 ppm at 52 km disagree with photochemical models such as Krasnopolsky (2012) and Rimmer et al. (2021). However, our results suggest that these measurements would be consistent with simulations assuming a PO flux above $1 \times 10^{10} \text{ molecules cm}^{-2} \text{ s}^{-1}$, which do not produce significant abiotic PH_3 . Above the clouds, photochemical models typically overestimate the upper limit O_2 concentrations of 3 ppm that is uniformly mixed above 58 km, as suggested by Mills (1999). Consistent with Yung et al. (2009); Krasnopolsky (2012); Zhang et al. (2012); Rimmer et al. (2021) for example, we find a strong increase in O_2 with concentrations higher than 10 ppm above 80 km.

An input flux of $5 \times 10^6 \text{ molecules cm}^{-2} \text{ s}^{-1} \text{ H}_3\text{PO}_4$ between 50 and 60 km leads to a maximum in the PH_3 concentration of 5×10^{-17} at 60 km. This result is comparable to the upper limit of abiotically produced PH_3 of about 2×10^{-16} from H_3PO_4 destruction in the Venus clouds found by Greaves et al. (2021a). Fluxes higher than $5 \times 10^6 \text{ molecules cm}^{-2} \text{ s}^{-1} \text{ H}_3\text{PO}_4$ lead to an increase in O_2 below 60 km and subsequent lower concentrations of PH_3 (not shown). Figures 4 and 5 suggest that the observed PH_3 concentrations of 1–4 ppb cannot be reproduced abiotically. A caveat of this result, however, is that it has not considered uncertainties in the model boundary conditions and in the rate coefficients of phosphorus-containing reactions. We therefore consider these uncertainties in the following section.

3.3. Uncertainties from the choice of boundary conditions

Figure 6 shows the dependence of PH_3 , PO , and H_3PO_4 on the choice of the SO_2 below the clouds for scenarios 1a, 1b, 2a, and 2b. We do not show the results for scenarios 1c and 2c because the simulated concentrations of SO_2 , H_2O , SO , and OCS above the clouds are not consistent with the concentrations that have been observed (see Sect. 3.1). The results suggest that the

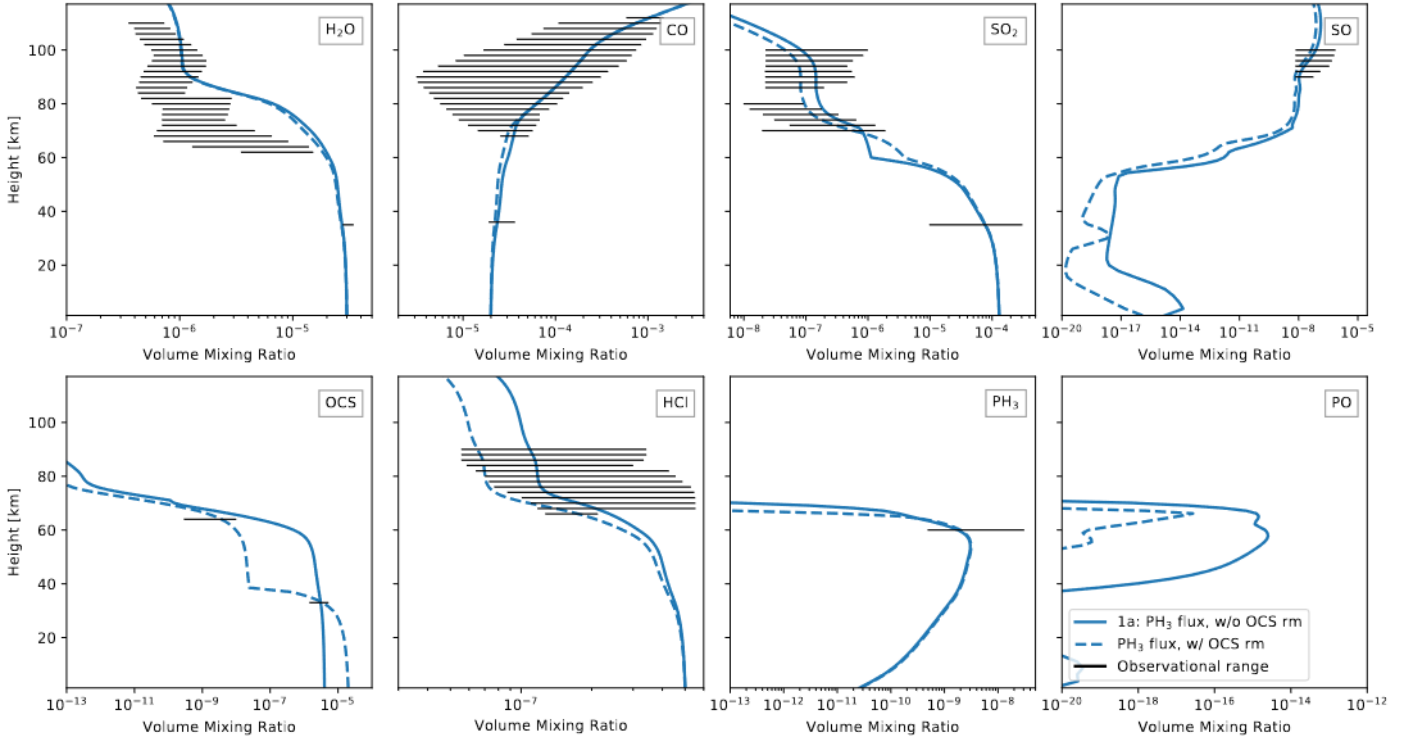


Fig. 3. As for Fig. 2, but comparing scenario 1a (solid blue line) with the same scenario, but with the additional sink for OCS in the clouds (see Sect. 3.1), (dashed blue line).

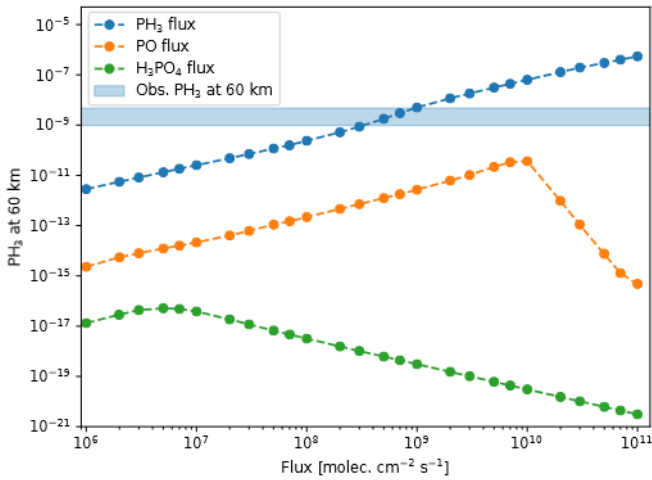


Fig. 4. Concentrations of PH_3 at 60 km for scenario 1a (blue dots and dashed line), scenario 2a (orange dots and dashed line), and scenario 3 (green dots and dashed line) with increasing input fluxes of PH_3 between 50 and 60 km, PO below 25 km, and H_3PO_4 between 50 and 60 km, respectively. The observational range of PH_3 is taken from Greaves et al. (2020).

scenarios with low SO_2 below the clouds feature stronger concentrations of PH_3 and PO than the runs with high SO_2 . For scenario 1a, the mixing ratio of PH_3 reaches a maximum of 3 ppb at around 55 km. Above 60 km, the predicted PH_3 drops off rapidly. In scenario 1b, a maximum of 4 ppb for PH_3 is reached at around 60 km, and the strong decrease in PH_3 occurs at around 70 km. This very short lifetime of PH_3 above the clouds is consistent with results from Greaves et al. (2021a).

In the cloud deck, the concentrations of PO are around 50 ppb for scenario 2a and 100 ppb for scenario 2b. The results

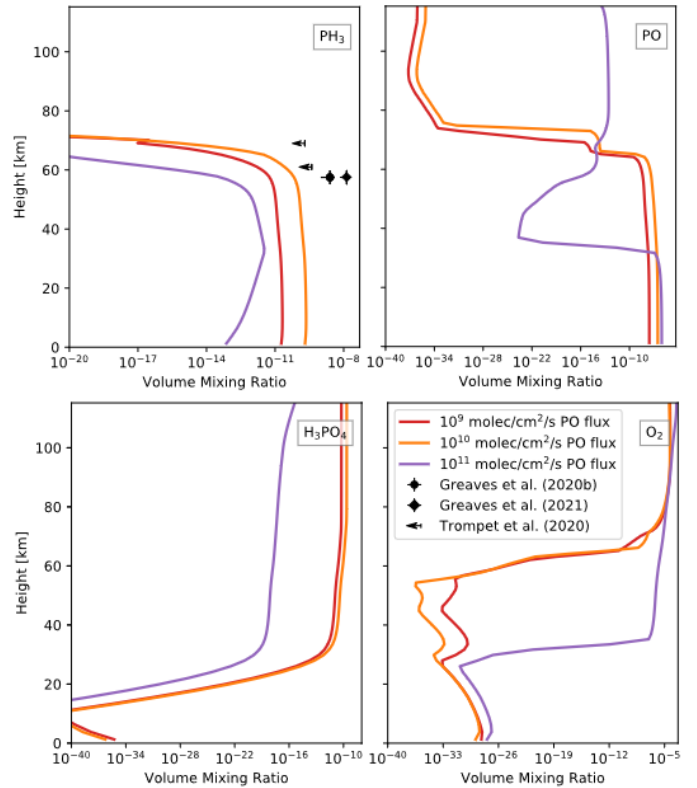


Fig. 5. Predicted volume mixing ratios of PH_3 , PO, H_3PO_4 , and O_2 against height for scenario 2a with three different PO input fluxes: 1×10^9 molecules $\text{cm}^{-2} \text{s}^{-1}$ (red line), 1×10^{10} molecules $\text{cm}^{-2} \text{s}^{-1}$ (orange line), and 1×10^{11} molecules $\text{cm}^{-2} \text{s}^{-1}$ (purple line). We additionally show the observational ranges from Greaves et al. (2020, 2021b) and upper limits of Trompet et al. (2021).

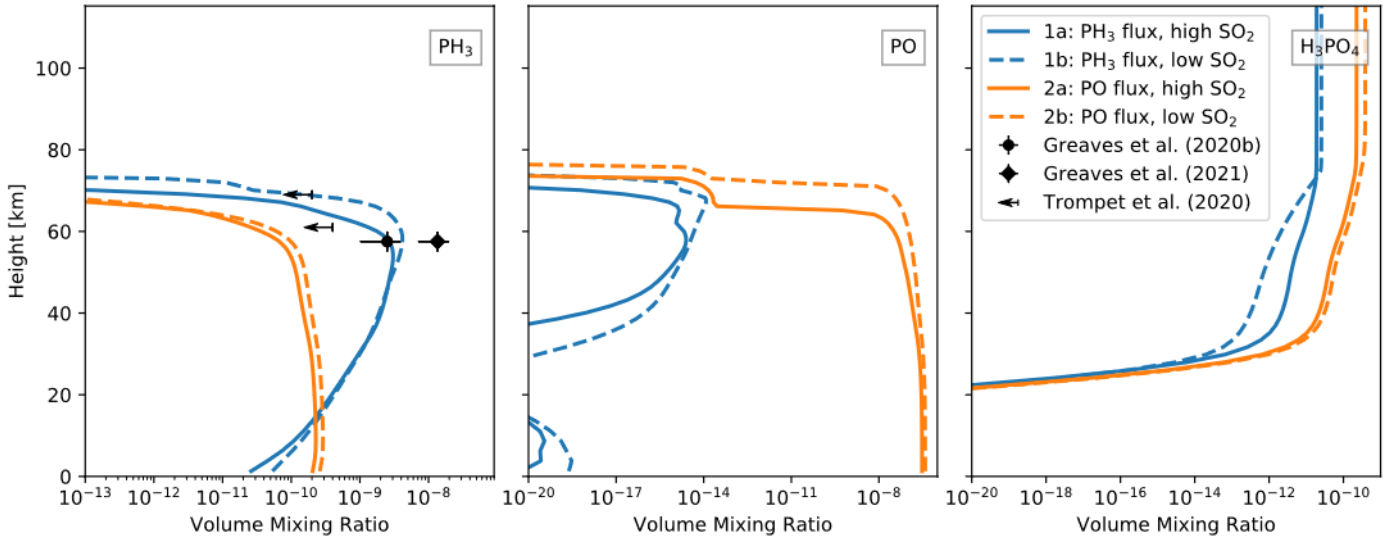


Fig. 6. Venus composition profiles for PH_3 , PO , and H_3PO_4 predicted with our photochemistry model for scenarios 1a (solid blue line), 1b (dashed blue line), 2a (solid orange line), and 2b (dashed orange line). We additionally show the observational ranges from Greaves et al. (2020, 2021b) and upper limits of Trompet et al. (2021).

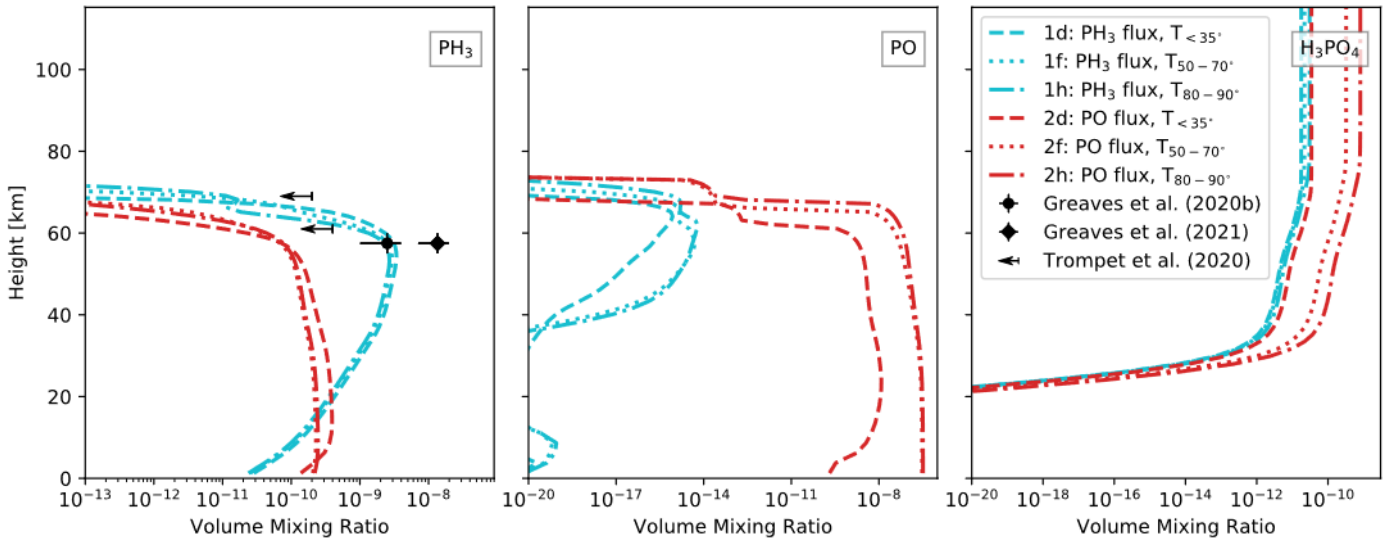


Fig. 7. As for Fig. 6, but showing the effect of varying the input temperature profile (see the legend).

for these scenarios suggest abiotically produced PH_3 concentrations between 0.1 and 0.3 ppb below 60 km, about one order of magnitude below the value observed by Greaves et al. (2020). The mixing ratios of PO below 60 km are lower by more than six orders of magnitude for scenarios 1a and 1b than in scenarios 2a and 2b. Hence, the concentrations of PO are well separated for the scenarios in which PH_3 originates from photochemistry and the scenarios in which PH_3 is directly injected with a fixed input flux. Thus, results suggest that observations of PO might provide useful constraints on the origin of PH_3 .

The concentrations of H_3PO_4 increase from the surface to the top of atmosphere. The model predicts that H_3PO_4 is the dominant phosphorus species above 70 km (see also Bains et al. 2021). H_3PO_4 shows larger abundances for scenarios 2a and 2b than for scenario 1a and 2b. The maximum mixing ratios of H_3PO_4 are higher by about one order of magnitude for the scenarios with chemically produced PH_3 than for the scenarios with a PH_3 input flux. Hence, without considering the uncertainties from the input temperature profile and rate coefficients (see

Sect. 3.4), the simulations suggest that a simultaneous detection of PH_3 and H_3PO_4 might (similar to the PO result just discussed) provide information on the origin of PH_3 .

Figure 7 shows the simulated mixing ratios of PH_3 , PO , and H_3PO_4 as a function of height using different input temperature profiles for the simulations with PH_3 fluxes (cyan lines) and PO fluxes (red lines). The choice of temperature profile below 60 km has little influence on the simulated concentrations of PH_3 , PO , and H_3PO_4 and other species for scenarios with a PH_3 flux (see also Fig. 2). The PH_3 concentrations at the cloud top show little dependence on the temperature profile for all scenarios.

For simulations with the PO flux, the concentration of PO is about two orders of magnitude lower when using the low-latitude temperature profile (scenario 2d) compared to scenarios 2f and 2h. The H_3PO_4 concentrations above the clouds is highest for the run with a PO flux using the high-latitude temperature profile (scenario 2h). When using the temperature profile for low-latitudes (scenario 2d), the volume mixing ratios of H_3PO_4 are similar to those in scenario 1h. Hence, when we consider

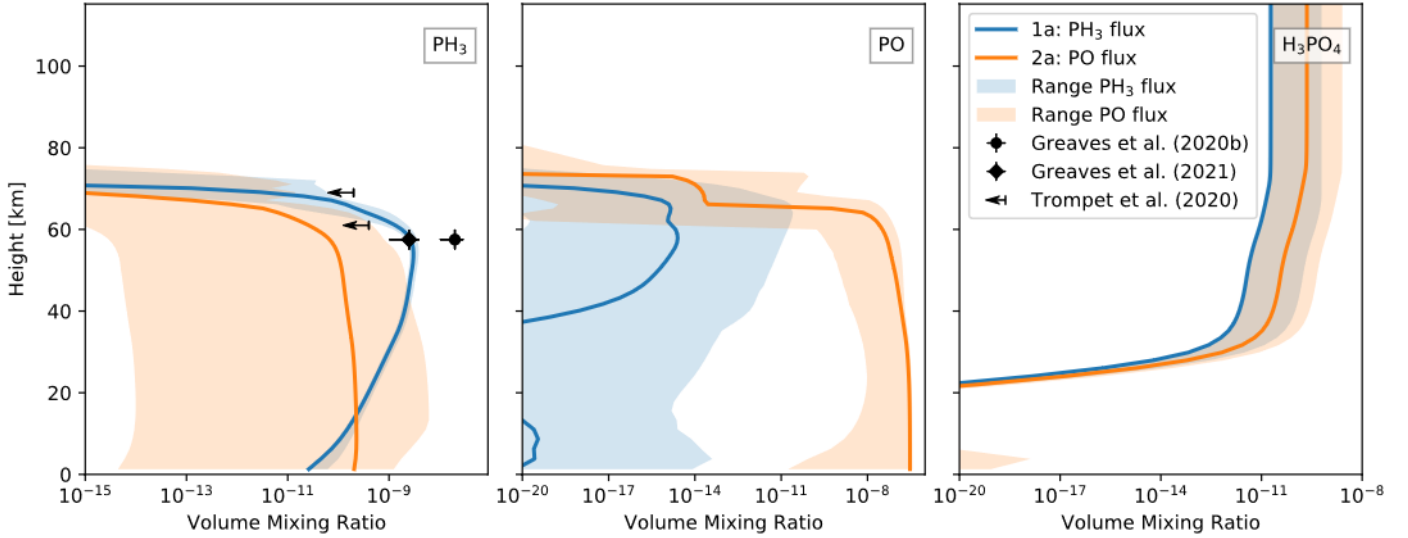


Fig. 8. Venus composition profiles for selected species predicted with our photochemistry model for scenario 1 (PH₃ flux, solid blue line) and scenario 2 (PO flux, solid orange line). The shaded areas show the 99% ranges of the MC runs of scenario 1 (shaded blue) and scenario 2 (shaded orange). For comparison, a range of observations is shown with black lines. We additionally show the observational ranges from Greaves et al. (2020, 2021b) and upper limits of Trompet et al. (2021).

the uncertainties from the temperature profile, the results suggest that it will be challenging to separate the scenarios with PH₃ fluxes from the scenarios with PO fluxes based on H₃PO₄ observations.

3.4. Uncertainties from rate coefficients

Figure 8 compares the chemical profiles of PH₃, PO, and H₃PO₄ from scenario 1a (shown in blue), assuming a PH₃ flux of 5×10^8 molecules cm⁻² s⁻¹ between 50 and 60 km with the results of scenario 2a (shown in orange), assuming a PO flux of 1×10^{10} molecules cm⁻² s⁻¹ below 25 km. The shaded blue and orange regions represent the 99% uncertainty range from the MC runs considering the uncertainties from using different temperature input profiles and the uncertainties of the PPN rate coefficients. The uncertainty range shows that up to 2 ppb PH₃ at 50 km, 1.5 ppb PH₃ at 55 km and 0.6 ppb PH₃ at 60 km can be produced abiotically. Our abiotic uncertainty range includes the upper limit of Trompet et al. (2021) with 0.4 ppb at 61 km and agrees with the planet-averaged abundances of PH₃ of 1–4 ppb between 55 and 60 km shown in Greaves et al. (2020). However, our abiotic upper limit is not consistent with the most recent estimate of 7 ppb PH₃ above 55 km suggested in Greaves et al. (2021b).

As discussed in Sect. 3.3, the choice of the temperature profile has only little effect on the abiotic production of PH₃. Figure 8 shows that the uncertainties from the estimated phosphorus rate coefficients are much larger. At 55 km, the range of the volume-mixing ratio of the abiotically produced PH₃ spans almost six orders of magnitude. On the other hand, the rate coefficients for reactions that destroy PH₃ are much better known. Hence, the uncertainty of PH₃ for the PH₃ flux scenarios is small, it ranges from 2.5 ppb to 3.8 ppb at 55 km.

The concentration ranges of PO for the runs considering a PH₃ input flux and a PO input flux do not overlap below 55 km. Hence, observations of PO could help to constrain whether PH₃ is produced by photochemistry or by other processes. Line lists and cross sections of PO have been computed by Prajapat et al. (2017) for instance. In this study, however, we limit our analysis

to the photochemical response of high PO concentrations and do not investigate the potential detectability of PO in the atmosphere of Venus.

Similar to PO (see Fig. 8), our results suggest that the uncertainty ranges for PO₂ (not shown) are separated for both sets of scenarios below 60 km. However, theoretical investigations suggest that PO₂ may not exist in the gas phase for conditions in the Venus clouds (see e.g. Haworth et al. 2002). If we do not consider PO₂ in our PPN, we find that the abundances of PO, H₃PO₄, and PH₃ are similar to the results shown in Fig. 8. The uncertainty ranges for H₃PO₄ for the scenarios with PH₃ input fluxes and PO input flux largely overlap. This suggests that a simultaneous detection of PH₃ and H₃PO₄ would not reveal information about the origin of PH₃.

4. Conclusions

We simulated the atmosphere of modern Venus with a sophisticated photochemical model including a new phosphorus reaction network in order to test the reproducibility of the observed concentrations of PH₃. We considered three sets of scenarios: first with input fluxes of PH₃ between 50–60 km, similar to the approach of Greaves et al. (2021a); second with input fluxes of PO below 25 km; and third with input fluxes of H₃PO₄ between 50–60 km. We considered the uncertainties of the temperature input profile and phosphorus reaction rate coefficients to compute a range of possible solutions with 200 MC runs for each of the scenarios. The main conclusions are listed below.

- Our study suggests that a PH₃ flux of 5×10^8 molecules cm⁻² s⁻¹ (4.1 Tg yr^{-1}) between 50 and 60 km is needed to reproduce a PH₃ mixing ratio of about 3 ppb at 60 km.
- The choice of the temperature profile and the SO₂ abundance in the lower atmosphere has little impact on the PH₃ concentrations in the Venus clouds.
- Varying H₃PO₄ fluxes between 50 and 60 km led to a maximum PH₃ mixing ratio of 5×10^{-17} at 60 km. This supports the results of Greaves et al. (2021a) and Bains et al. (2021) that a significant photochemical production of PH₃ from H₃PO₄ pathways is unlikely.

- We find that volume mixing ratios of PH₃ between 1×10^{-15} and 2×10^{-9} might be produced abiotically at the height of the Venus clouds when assuming a PO input flux of 1×10^{10} molecules cm⁻² s⁻¹ (113 Tg yr⁻¹) below 25 km.
- The production of PO from destruction of PH₃ is only weak (scenarios 1a–1h). Hence, the detection of large abundances of PO and PH₃ might be an indicator for an abiotic production of PH₃ via PO pathways.

Our main conclusion is that we can reproduce the lower estimates of about 1 ppb PH₃ claimed by Greaves et al. (2020) in the Venus clouds with abiotic sources of PH₃ alone when we take into account the uncertainties in the chemical rate coefficients.

Acknowledgements. The authors acknowledge the support of the DFG priority program SPP 1992 “Exploring the Diversity of Extrasolar Planets”.

References

- Akins, A. B., Lincowski, A. P., Meadows, V. S., & Steffes, P. G. 2021, *ApJ*, **907**, L27
- Arthur, N. L., & Cooper, I. A. 1997, *J. Chem. Soc., Faraday Trans.*, **93**, 521
- Bains, W., Petkowski, J. J., Sousa-Silva, C., & Seager, S. 2019, *Sci. Total Environ.*, **658**, 521
- Bains, W., Petkowski, J. J., Seager, S., et al. 2021, *Astrobiology*, **21**, 1277
- Bains, W., Shorttle, O., Ranjan, S., et al. 2022, *PNAS*, **119**, e2121702119
- Baulch, D., Cobos, C., Cox, R., et al. 1995, *J. Phys. Chem. Ref. Data*, **23**, 847
- Belyaev, D. A., Montmessin, F., Bertaux, J.-L., et al. 2012, *Icarus*, **217**, 740
- Bertaux, J.-L., Widemann, T., Hauchecorne, A., Moroz, V. I., & Ekonomov, A. P. 1996, *J. Geophys. Res.: Planets*, **101**, 12709
- Bertaux, J.-L., Vandaele, A.-C., Korabiev, O., et al. 2007, *Nature*, **450**, 646
- Bolshova, T., & Korobeinichev, O. 2006, *Combust. Explos. Shock Waves*, **42**, 493
- Bosco, S. R., Brobst, W. D., Nava, D. F., & Stief, L. J. 1983, *JGR*, **88**, 8543
- Bozzelli, J. W., & Dean, A. M. 1989, *J. Phys. Chem.*, **93**, 1058
- Bézard, B., de Bergh, C., Fegley, B., et al. 1993, *Geophys. Res. Lett.*, **20**, 1587
- Chen, F., Judge, D. L., Robert Wu, C. Y., et al. 1991, *JGR: Planets*, **96**, 17519
- Clyne, M. A. A., & Ono, Y. 1982, *J. Chem. Soc., Faraday Trans. 2*, **78**, 1149
- Cohen, N., & Westberg, K. R. 1991, *J. Phys. Chem. Ref. Data*, **20**, 1211
- DeMore, W. B., Margitan, J. J., Molina, M. J., et al. 1985, *Int. J. Chem. Kinetics*, **17**, 1135
- Encrenaz, T., Greathouse, T. K., Marcq, E., et al. 2020, *A&A*, **643**, A5
- Fontijn, A., Shamsuddin, S. M., Crammond, D., Marshall, P., & Anderson, W. R. 2006, *Combust. Flame*, **145**, 543
- Fritz, B., Lorenz, K., Steinert, W., & Zellner, R. 1982, in *Phys. Chem. Behav. Atmos. Pollut. Proc. Eur. Symp.*, 192
- Greaves, J. S., Richards, A. M. S., Bains, W., et al. 2020, ArXiv e-prints [arXiv:2011.08176]
- Greaves, J. S., Richards, A. M. S., Bains, W., et al. 2021a, *Nat. Astron.*, **5**, 655
- Greaves, J. S., Richards, A. M. S., Bains, W., et al. 2021b, *Nat. Astron.*, **5**, 636
- Greaves, J. S., Rimmer, P. B., Richards, A. M. S., et al. 2022, *MNRAS*, **514**, 2994
- Hamilton, P. A., & Murrells, T. P. 1985, *J. Chem. Soc., Faraday Trans. 2*, **81**, 1531
- Haus, R., Kappel, D., & Arnold, G. 2013, *Planet. Space Sci.*, **89**, 77
- Haworth, N. L., Bacskay, G. B., & Mackie, J. C. 2002, *J. Phys. Chem. A*, **106**, 1533
- Henshaw, T. L., MacDonald, M. A., Stedman, D. H., & Coombe, R. D. 1987, *J. Phys. Chem.*, **91**, 2838
- Higashihara, T., Saito, K., & Murakami, I. 1978, *Bull. Chem. Soc. Jpn.*, **51**, 3426
- Iyer, R. S., Rogers, P. J., & Rowland, F. 1983, *J. Phys. Chem.*, **87**, 3799
- Kaye, J. A., & Strobel, D. F. 1984, *Icarus*, **59**, 314
- Koshi, M., Yoshimura, M., Fukuda, K., et al. 1990, *J. Chem. Phys.*, **93**, 8703
- Krasnopolsky, V. 1989, *Icarus*, **80**, 202
- Krasnopolsky, V. A. 2007, *Icarus*, **191**, 25
- Krasnopolsky, V. A. 2010, *Icarus*, **209**, 314
- Krasnopolsky, V. A. 2012, *Icarus*, **218**, 230
- Krasnopolsky, V. A. 2013, *Icarus*, **225**, 570
- Krasnopolsky, V., & Parshev, V. 1981, *Nature*, **292**, 610
- Lincowski, A. P., Meadows, V. S., Crisp, D., et al. 2021, *ApJ*, **908**, L44
- Mallard, W., Westley, F., Herron, J., Hampson, R., & Frizzell, D. 1994, *NIST Chemical Kinetics Database, Ver. 6.0*. (Gaithersburg, MD: National Institute of Standards and Technology)
- Marcq, E., Bézard, B., Drossart, P., et al. 2008, *J. Geophys. Res.: Planets*, **113**
- Marcq, E., Mills, F. P., Parkinson, C. D., & Vandaele, A. C. 2018, *Space Sci. Rev.*, **214**, 10
- McTaggart, R. 2022, *Icarus*, **374**, 114791
- Mills, F. P. 1999, *J. Geophys. Res.: Planets*, **104**, 30757
- Nava, D. F., & Stief, L. J. 1989, *J. Phys. Chem.*, **93**, 4044
- Omran, A., Oze, C., Jackson, B., et al. 2021, *Astrobiology*, **21**, 1264
- Oyama, V. I., Carle, G. C., Woeller, F., & Pollack, J. B. 1979, *Science*, **203**, 802
- Patel, M., Mason, J., Nordheim, T., & Dartnell, L. 2022, *Icarus*, **373**, 114796
- Pollack, J. B., Dalton, J., Grinspoon, D., et al. 1993, *Icarus*, **103**, 1
- Prajapat, L., Jagoda, P., Lodi, L., et al. 2017, *MNRAS*, **472**, 3648
- Rimmer, P. B., Jordan, S., Constantinou, T., et al. 2021, *Planet. Sci. J.*, **2**, 133
- Röhrig, M., & Wagner, H. G. 1994, *Symp. (Int.) Combust.*, **25**, 975
- Römming, H.-J., & Wagner, H. 1996, *Symp. (Int.) Combust.*, **26**, 559
- Sandor, B. J., & Clancy, R. T. 2012, *Icarus*, **220**, 618
- Sandor, B. J., Clancy, R. T., Moriarty-Schieven, G., & Mills, F. P. 2010, *Icarus*, **208**, 49
- Sausa, R. C., Miziolek, A. W., & Long, S. R. 1986, *J. Phys. Chem.*, **90**, 3994
- Scheucher, M., Wunderlich, F., Grenfell, J. L., et al. 2020, *ApJ*, **898**, 44
- Snellen, I. A. G., Guzman-Ramirez, L., Hogerheijde, M. R., Hygate, A. P. S., & van der Tak, F. F. S. 2020, *A&A*, **644**, A2
- Sousa-Silva, C., Seager, S., Ranjan, S., et al. 2020, *Astrobiology*, **20**, 235
- Sullivan, P. A., Sumathi, R., Green, W. H., & Tester, J. W. 2004, *Phys. Chem. Chem. Phys.*, **6**, 4296
- Svedhem, H., Titov, D. V., Taylor, F. W., & Witasse, O. 2007, *Natur*, **450**, 629
- Thompson, M. A. 2021, *MNRAS*, **501**, L18
- Trompet, L., Robert, S., Mahieux, A., et al. 2021, *A&A*, **645**, A4
- Truong, N., & Lunine, J. I. 2021, *PNAS*, **118**, e2021689118
- Tsang, W., & Herron, J. T. 1991, *J. Phys. Chem. Ref. Data*, **20**, 609
- Vahedpour, M., Douroudgari, H., Afshar, S., & Asgharzade, S. 2018, *Chem. Phys.*, **507**, 51
- Villanueva, G., Cordiner, M., Irwin, P., et al. 2021, *Nat. Astron.*, **5**, 631
- Wang, S., Hu, Z., Zhang, J., et al. 2022, *Environ. Technol. Innov.*, **28**, 102653
- Wunderlich, F., Scheucher, M., Godolt, M., et al. 2020, *ApJ*, **901**, 126
- Wunderlich, F., Scheucher, M., Grenfell, J. L., et al. 2021, *A&A*, **647**, A48
- Yung, Y. L., Liang, M. C., Jiang, X., et al. 2009, *J. Geophys. Res.: Planets*, **114**
- Zhang, X., Liang, M. C., Mills, F. P., Belyaev, D. A., & Yung, Y. L. 2012, *Icarus*, **217**, 714

Appendix A: Phosphorus network

Table A.1. Phosphorus-containing reactions added to the original BLACKWOLF photochemical reaction scheme from Wunderlich et al. (2020).

Number	Reactions	Reaction Coefficients	References	Notes
R1	$\text{PH}_3 + \text{Cl} \rightarrow \text{PH}_2 + \text{HCl}$	2.36×10^{-10}	(1)	
R2	$\text{PH}_3 + \text{N} \rightarrow \text{PH}_2 + \text{NH}$	4.00×10^{-14}	(2)	
R3	$\text{PH}_3 + \text{O} \rightarrow \text{PH}_2 + \text{OH}$	4.75×10^{-11}	(3)	
R4	$\text{PH}_3 + \text{NH}_2 \rightarrow \text{PH}_2 + \text{NH}_3$	$1.50 \times 10^{-12} \cdot e^{-928.0/T}$	(4)	
R5	$\text{PH}_3 + \text{H} \rightarrow \text{PH}_2 + \text{H}_2$	$7.22 \times 10^{-11} \cdot e^{-886.0/T}$	(5)	
R6	$\text{PH}_3 + \text{OH} \rightarrow \text{PH}_2 + \text{H}_2\text{O}$	$2.71 \times 10^{-11} \cdot e^{-155.0/T}$	(6)	
R7	$\text{PH}_3 + \text{M} \rightarrow \text{PH}_2 + \text{H} + \text{M}$	$k_0 = 3.4 \times 10^{-8} \cdot e^{-35644.0/T}$ $k_\infty = 1.91 \times 10^{18} \cdot e^{-40063.0/T}$	(7)	
R8	$\text{PH}_3 + h\nu \rightarrow \text{PH}_2 + \text{H}$	see table notes	(8)	
R9	$\text{PH}_2 + \text{H} + \text{M} \rightarrow \text{PH}_3 + \text{M}$	$3.7 \times 10^{-10} \cdot e^{-340.0/T}$	(9)	
R10	$\text{PH} + \text{H}_2 + \text{M} \rightarrow \text{PH}_3 + \text{M}$	$3.00 \times 10^{-36} \cdot N$	(9)	
R11	$\text{PH}_2 + \text{H} \rightarrow \text{PH} + \text{H}_2$	$6.20 \times 10^{-11} \cdot e^{-318.0/T}$	(9)	
R12	$\text{PH} + \text{H} \rightarrow \text{P} + \text{H}_2$	$1.5 \times 10^{-10} \cdot e^{-416.0/T}$	(9)	
R13	$\text{P} + \text{H} + \text{M} \rightarrow \text{PH} + \text{M}$	$3.4 \times 10^{-33} \cdot e^{173.0/T} \cdot N$	(9)	
R14	$\text{H}_3\text{PO}_4 + \text{H} \rightarrow \text{H}_2\text{PO}_3 + \text{H}_2\text{O}$	$1.19 \times 10^{-11} \cdot (T/298.0)^{1.69} \cdot e^{-19123.3/T}$	(10)	
R15	$\text{H}_3\text{PO}_4 + \text{H} + \text{M} \rightarrow \text{H}_4\text{PO}_4 + \text{M}$	$1.08 \times 10^{-12} \cdot (T/298.0)^{2.07} \cdot e^{-10955.6/T}$	(10)	
R16	$\text{H}_3\text{PO}_4 + \text{M} \rightarrow \text{HPO}_3 + \text{H}_2\text{O} + \text{M}$	$8.6 \times 10^{10} \cdot (T/298.0)^{1.46} \cdot e^{-21167.9/T}$	(10)	
R17	$\text{H}_4\text{PO}_4 + \text{M} \rightarrow \text{H}_2\text{PO}_3 + \text{H}_2\text{O} + \text{M}$	$2.86 \times 10^{11} \cdot (T/298.0)^{0.91} \cdot e^{-13590.8/T}$	(10)	
R18	$\text{H}_2\text{PO}_3 + \text{H} \rightarrow \text{HPO}_2 + \text{H}_2\text{O}$	$1.05 \times 10^{-12} \cdot e^{-6007.6/T}$	(11)	(+)
R19	$\text{H}_2\text{PO}_3 + \text{O}_2 \rightarrow \text{HPO}_3 + \text{HO}_2$	$1.87 \times 10^{-16} \cdot (T/298.0)^{2.4} \cdot e^{-211.7/T}$	(10)	
R20	$\text{HPO}_3 + \text{H} + \text{M} \rightarrow \text{H}_2\text{PO}_3 + \text{M}$	$4.18 \times 10^{-12} \cdot (T/298.0)^{1.58} \cdot e^{-3115.1/T}$	(10)	
R21	$\text{HPO}_3 + \text{M} \rightarrow \text{PO}_2 + \text{OH} + \text{M}$	$2.01 \times 10^{18} \cdot (T/298.0)^{-2.48} \cdot e^{-56407.7/T}$	(12)	(+)
R22	$\text{HPO}_3 + \text{H} \rightarrow \text{PO}_2 + \text{H}_2\text{O}$	$1.05 \times 10^{-12} \cdot e^{-6007.6/T}$	(11)	(+)
R23	$\text{PO}_2 + \text{OH} + \text{M} \rightarrow \text{HPO}_3 + \text{M}$	$26.6 \cdot T^{-2.3} \cdot e^{-143.1/T}$	(11)	(+)
R24	$\text{PO}_2 + \text{H} + \text{M} \rightarrow \text{HPO}_2 + \text{M}$	$16.2 \cdot T^{-2.0} \cdot e^{-324.7/T}$	(11)	(+)
R25	$\text{HPO}_2 + \text{M} \rightarrow \text{PO}_2 + \text{H} + \text{M}$	$1.89 \times 10^{22} \cdot (T/298.0)^{-5.13} \cdot e^{-48349.4/T}$	(12)	(+)
R26	$\text{HPO}_2 + \text{H} \rightarrow \text{PO}_2 + \text{H}_2$	$1.31 \times 10^{-12} \cdot e^{-21.6/T}$	(11)	(+)
R27	$\text{PO} + \text{O}_2 \rightarrow \text{PO}_2 + \text{O}$	1.20×10^{-11}	(13)	
R28	$\text{HPO}_2 + \text{OH} \rightarrow \text{PO}_2 + \text{H}_2\text{O}$	5.25×10^{-13}	(11)	(+)
R29	$\text{HPO}_2 + \text{H} \rightarrow \text{PO} + \text{H}_2\text{O}$	$1.05 \times 10^{-12} \cdot e^{-6007.6/T}$	(11)	(+)
R30	$\text{P} + \text{NO}_2 \rightarrow \text{PO} + \text{NO}$	1.60×10^{-11}	(14)	
R31	$\text{P} + \text{O}_2 \rightarrow \text{PO} + \text{O}$	1.10×10^{-13}	(15)	
R32	$\text{HPO}_3 + \text{O} \rightarrow \text{HPO}_2 + \text{O}_2$	$1.03 \times 10^{-12} \cdot e^{-4147.0/T}$	(11)	(+)
R33	$\text{PO}_2 + \text{H} \rightarrow \text{PO} + \text{OH}$	$4.0 \times 10^{-10} \cdot e^{-340.0/T}$	(16)	(*)
R34	$\text{HPO} + \text{OH} \rightarrow \text{PO} + \text{H}_2\text{O}$	$8.0 \times 10^{-11} \cdot e^{-500.0/T}$	(17)	(*)
R35	$\text{PO} + \text{H} + \text{M} \rightarrow \text{HPO} + \text{M}$	$k_0 = 1.34 \times 10^{-31} \cdot (T/298.0)^{-1.32} \cdot e^{-370.5/T}$ $k_\infty = 2.44 \times 10^{-10} \cdot (T/298.0)^{-0.41}$	(17)	(*)
R36	$\text{PO} + \text{H}_2 \rightarrow \text{HPO} + \text{H}$	$2.31 \times 10^{-11} \cdot e^{-28384.2/T}$	(17)	(*)
R37	$\text{PO} + \text{O} \rightarrow \text{P} + \text{O}_2$	$8.93 \times 10^{-13} \cdot (T/298.0)^{1.0} \cdot e^{-19484.1/T}$	(17)	(*)
R38	$\text{PO} + \text{H} \rightarrow \text{P} + \text{OH}$	$2.81 \times 10^{-10} \cdot e^{-24655.8/T}$	(17)	(*)
R39	$\text{HPO} + \text{H} \rightarrow \text{PO} + \text{H}_2$	$3.0 \times 10^{-11} \cdot e^{-500.0/T}$	(17)	(*)
R40	$\text{HPO} + \text{M} \rightarrow \text{PO} + \text{H} + \text{M}$	$k_0 = 5.48 \times 10^{-7} \cdot (T/298.0)^{-1.24} \cdot e^{-25257.1/T}$ $k_\infty = 1.04 \times 10^{15} \cdot (T/298.0)^{-1.61} \cdot e^{-24896.3/T}$	(17)	(*)
R41	$\text{PO} + \text{H} \rightarrow \text{PH} + \text{O}$	$9.3 \times 10^{-10} \cdot (T/298.0)^{-0.1} \cdot e^{-5239.8/T}$	(18)	(*)
R42	$\text{HPO} + \text{H} \rightarrow \text{PH}_2 + \text{O}$	$1.05 \times 10^{-9} \cdot (T/298.0)^{-0.3} \cdot e^{-14673.2/T}$	(18)	(*)
R43	$\text{HPO} + \text{H} \rightarrow \text{PH} + \text{OH}$	$2.41 \times 10^{-9} \cdot (T/298.0)^{-0.5} \cdot e^{-9010.0/T}$	(18)	(*)
R44	$\text{P} + \text{H}_2 \rightarrow \text{PH} + \text{H}$	$4.65 \times 10^{-10} \cdot e^{-16597.6/T}$	(19)	(*)
R45	$\text{PH} + \text{OH} \rightarrow \text{PH}_2 + \text{O}$	$2.94 \times 10^{-12} \cdot (T/298.0)^{0.1} \cdot e^{-5800.0/T}$	(18)	(*)
R46	$\text{PH} + \text{H}_2 \rightarrow \text{PH}_2 + \text{H}$	$3.5 \times 10^{-11} \cdot e^{-7757.6/T}$	(20)	(*)
R47	$\text{H}_2\text{PO}_3 + \text{OH} \rightarrow \text{HPO}_3 + \text{H}_2\text{O}$	5.25×10^{-13}	(11)	(+)
R48	$\text{H}_2\text{PO}_3 + \text{M} \rightarrow \text{PO}_2 + \text{H}_2\text{O} + \text{M}$	$1.66 \times 10^{-12} \cdot e^{-15082.1/T} \cdot N$	(11)	(+)
R49	$\text{H}_2\text{PO}_3 + \text{OH} + \text{M} \rightarrow \text{H}_3\text{PO}_4 + \text{M}$	$26.6 \cdot T^{-2.3} \cdot e^{-143.1/T}$	(11)	(+)
R50	$\text{PO} + \text{OH} + \text{M} \rightarrow \text{HPO}_2 + \text{M}$	$1.98 \times 10^{-4} \cdot T^{-1.8} \cdot e^{-700.0/T}$	(11)	(+)
R51	$\text{HPO}_2 + \text{O} \rightarrow \text{PO}_2 + \text{OH}$	2.62×10^{-12}	(11)	(+)

Table A.1: continued.

Number	Reactions	Reaction Coefficients	References	Notes
R52	$\text{PO} + \text{OH} \rightarrow \text{PO}_2 + \text{H}$	$1.05 \times 10^{-13} \cdot e^{-3000.8/T}$	(11)	(+)
R53	$\text{PO} + \text{O} + \text{M} \rightarrow \text{PO}_2 + \text{M}$	$3.92 \cdot T^{-2.1} \cdot e^{-556.9/T}$	(11)	(+)
R54	$\text{HPO}_2 + \text{OH} \rightarrow \text{HPO}_3 + \text{H}$	$1.05 \times 10^{-13} \cdot e^{-4895.1/T}$	(11)	(+)
R55	$\text{HPO}_2 + \text{O} + \text{M} \rightarrow \text{HPO}_3 + \text{M}$	$13.2 \cdot T^{-2.1} \cdot e^{-501.5/T}$	(11)	(+)
R56	$\text{HPO}_3 + \text{PO} \rightarrow \text{HPO}_2 + \text{PO}_2$	$5.25 \times 10^{-13} \cdot e^{-4904.7/T}$	(11)	(+)
R57	$\text{H}_3\text{PO}_3 + \text{OH} \rightarrow \text{H}_2\text{PO}_3 + \text{H}_2\text{O}$	5.25×10^{-13}	(21)	(+)
R58	$\text{H}_3\text{PO}_3 + \text{H} \rightarrow \text{H}_2\text{PO}_2 + \text{H}_2\text{O}$	$1.05 \times 10^{-12} \cdot e^{-6007.6/T}$	(22)	(+)
R59	$\text{H}_3\text{PO}_3 + \text{M} \rightarrow \text{HPO}_2 + \text{H}_2\text{O} + \text{M}$	$8.6 \times 10^{10} \cdot (T/298.0)^{1.46} \cdot e^{-21167.9/T}$	(23)	(*)
R60	$\text{H}_2\text{PO}_2 + \text{OH} \rightarrow \text{HPO}_2 + \text{H}_2\text{O}$	5.25×10^{-13}	(21)	(+)
R61	$\text{H}_2\text{PO}_2 + \text{H} \rightarrow \text{HPO} + \text{H}_2\text{O}$	$1.05 \times 10^{-12} \cdot e^{-6007.6/T}$	(22)	(+)
R62	$\text{H}_2\text{PO}_2 + \text{M} \rightarrow \text{PO} + \text{H}_2\text{O} + \text{M}$	$8.6 \times 10^{10} \cdot (T/298.0)^{1.46} \cdot e^{-21167.9/T}$	(23)	(*)
R63	$\text{HPO} + \text{O} \rightarrow \text{PO} + \text{OH}$	5.99×10^{-11}	(17)	(*)
R64	$\text{HPO} + \text{OH} \rightarrow \text{PO} + \text{H}_2\text{O}$	$8.0 \times 10^{-11} \cdot e^{-500.3/T}$	(17)	(*)
R65	$\text{PH} + \text{O}_2 \rightarrow \text{PO} + \text{OH}$	$6.74 \times 10^{-14} \cdot (T/298.0)^{0.79} \cdot e^{-601.4/T}$	(24)	(*)
R66	$\text{PH} + \text{O} \rightarrow \text{PO} + \text{H}$	1.16×10^{-10}	(18)	(*)
R67	$\text{PH}_2 + \text{O} \rightarrow \text{HPO} + \text{H}$	7.47×10^{-11}	(18)	(*)
R68	$\text{PH}_2 + \text{O}_2 \rightarrow \text{HPO} + \text{OH}$	$2.72 \times 10^{-13} \cdot (T/298.0)^{-0.39} \cdot e^{-18161.1/T}$	(25)	(*)
R69	$\text{PH}_2 + \text{OH} \rightarrow \text{HPO} + \text{H}_2$	$3.69 \times 10^{-13} \cdot (T/298.0)^{0.88} \cdot e^{-9091.4/T}$	(26)	(*)
R70	$\text{PH} + \text{O}_2 \rightarrow \text{HPO} + \text{O}$	$6.51 \times 10^{-11} \cdot e^{-9000.0/T}$	(27)	(*)
R71	$\text{PH} + \text{OH} \rightarrow \text{HPO} + \text{H}$	3.32×10^{-11}	(18)	(*)
R72	$\text{HPO}_2 + \text{OH} + \text{M} \rightarrow \text{H}_2\text{PO}_3 + \text{M}$	$1.98 \times 10^{-4} \cdot T^{-1.8} \cdot e^{-700.0/T}$	(28)	(+)
R73	$\text{HPO}_2 + \text{H} + \text{M} \rightarrow \text{H}_2\text{PO}_2 + \text{M}$	$k_0 = 1.34 \times 10^{-31} \cdot (T/298.0)^{-1.32} \cdot e^{-370.5/T}$ $k_\infty = 2.44 \times 10^{-10} \cdot (T/298.0)^{-0.41}$	(29)	(*)
R74	$\text{H}_2\text{PO}_2 + \text{OH} + \text{M} \rightarrow \text{H}_3\text{PO}_3 + \text{M}$	$1.98 \times 10^{-4} \cdot T^{-1.8} \cdot e^{-700.0/T}$	(28)	(+)
R75	$\text{H}_2\text{PO}_3 + \text{H} + \text{M} \rightarrow \text{H}_3\text{PO}_3 + \text{M}$	$k_0 = 1.34 \times 10^{-31} \cdot (T/298.0)^{-1.32} \cdot e^{-370.5/T}$ $k_\infty = 2.44 \times 10^{-10} \cdot (T/298.0)^{-0.41}$	(29)	(*)
R76	$\text{PO}_2 + \text{M} \rightarrow \text{PO} + \text{O} + \text{M}$	$k_0 = 1.88 \times 10^{-4} \cdot (T/298.0)^{-3.37} \cdot e^{-37645.2/T}$ $k_\infty = 5.48 \times 10^{15} \cdot (T/298.0)^{-1.27} \cdot e^{-37404.7/T}$	(17)	(*)
R77	$\text{PO}_2 + \text{O} \rightarrow \text{PO} + \text{O}_2$	$6.51 \times 10^{-12} \cdot e^{-120.0/T}$	(17)	(*)
R78	$\text{PO} + \text{HCl} \rightarrow \text{HPO} + \text{Cl}$	$2.62 \times 10^{-11} \cdot e^{-25257.2/T}$	(30)	(*)
R79	$\text{HPO} + \text{CO} \rightarrow \text{PH} + \text{CO}_2$	$3.32 \times 10^{-12} \cdot e^{-6190.4/T}$	(31)	(*)

Notes. The asterisk indicates missing rate data where phosphorus atoms present in reactant species are analogously replaced with nitrogen atoms for which rate data are available. The plus indicates reactions for which the rate data is only available for temperatures higher than 750 K. Bimolecular reaction coefficients are shown in $\text{cm}^3 \text{s}^{-1}$ and termolecular reactions are given in $\text{cm}^6 \text{s}^{-1}$. The unit of temperature, T , is K, and the unit of the number density, N , is cm^{-3} . Photolysis cross sections are taken from [Chen et al. \(1991\)](#) between 120 and 230 nm. The quantum yield is assumed to be unity.

References. (1) [Iyer et al. \(1983\)](#); (2) [Hamilton & Murrells \(1985\)](#); (3) [Nava & Stief \(1989\)](#); (4) [Bosco et al. \(1983\)](#); (5) [Arthur & Cooper \(1997\)](#); (6) [Fritz et al. \(1982\)](#); (7) [Greaves et al. \(2021a\)](#); (8) [Chen et al. \(1991\)](#); (9) [Kaye & Strobel \(1984\)](#); (10) [Sullivan et al. \(2004\)](#); (11) [Bolshova & Korobeinichev \(2006\)](#); (12) [Haworth et al. \(2002\)](#); (13) [Sausa et al. \(1986\)](#); (14) [Clyne & Ono \(1982\)](#); (15) [Henshaw et al. \(1987\)](#); (16) [DeMore et al. \(1985\)](#); (17) [Tsang & Herron \(1991\)](#); (18) [Cohen & Westberg \(1991\)](#); (19) [Koshi et al. \(1990\)](#); (20) [Fontijn et al. \(2006\)](#); (21) assumed same as R47; (22) assumed same as R18; (23) assumed same as R16; (24) [Römming & Wagner \(1996\)](#); (25) [Bozzelli & Dean \(1989\)](#); (26) [Vahedpour et al. \(2018\)](#); (27) [Baulch et al. \(1995\)](#); (28) assumed same as R50; (29) assumed same as R35; (30) [Higashihara et al. \(1978\)](#); (31) [Röhrig & Wagner \(1994\)](#)

Appendix B: Uncertainty distribution

The uncertainties in the chemical rate coefficients are fitted to log-normal distributions for which the standard deviation is derived. The phosphorus-containing reactions shown in Table A.1 are grouped into three types as follows:

1. Phosphorus reactions for which rate coefficient data are measured or valid for temperatures below 750 K (approximated surface temperature of Venus). For this type of reaction, we did not consider uncertainties in the rate coefficient data.
2. Phosphorus reactions for which rate coefficient data are not valid for temperatures below 750 K. These reactions are marked with a plus in Table A.1, and the uncertainties in their rate coefficient data were considered.
3. Reactions for which analogous rate coefficient data only exist for cases in which phosphorus is replaced with nitrogen. These reactions are marked with an asterisk in Table A.1, and the uncertainties in the rate coefficient data were considered.

For each MC run and each type 2 and type 3 reaction, we calculated a random factor inside the log-normal distribution and multiplied this factor with the rate coefficients of the reactions. The PPN used to simulate the phosphorus chemistry in this study includes type 2 reactions even when the observed rate coefficients are applied beyond their validity range for temperatures in the atmosphere of Venus. To estimate the uncertainty on extrapolating the coefficient data to Venus conditions, we collected all rate data from multiple studies over different reference temperature ranges. To be considered in our study, we specified that at least one of these data must be valid below temperatures of 750 K and at least one must be valid above 750 K. For the phosphorus-containing reactions R14, R16, and R27, rate coefficient data from Bolshova & Korobeinichev (2006) exist, in addition to the coefficients shown in Table A.1. To increase the number of members of the statistical analysis, we considered five nitrogen-containing reactions (analogue nitrogen reactions to R3, R5, R6, R21, and R53), where the rate data were taken from the National Institute of Standards and Technology (NIST, Mallard et al. 1994).

Note that datapoints in Fig. B.1 were constructed from the reactions in Table A.1 which are not marked with a plus. For these reactions, rate coefficient expressions exist which are valid below 750 K (as shown in Table A.1). Rate coefficient expressions also exist (see references in Table A.1) which are valid above 750 K. For every reaction, we calculated the coefficients between 200 and 750 K in 10 K steps. Then, for each reaction and temperature step, we divided the coefficients that are valid below 750 K ($C_{T_{\text{val}} < 750 \text{ K}}$) by the coefficients that are valid above 750 K ($C_{T_{\text{val}} > 750 \text{ K}}$). The logarithm of the reaction coefficient quotients was then fitted to a normal distribution. Three-body and thermolysis reaction coefficients can be very small for low temperatures and the difference between $C_{T_{\text{val}} < 750 \text{ K}}$ and $C_{T_{\text{val}} > 750 \text{ K}}$ can be more than ten orders of magnitude. However, these reactions are not expected to significantly influence the photochemistry in and above the Venus clouds. Hence, in order to avoid an overestimation of the uncertainty range, we used only $-10 < \log_{10}(C_{T_{\text{val}} < 750 \text{ K}} / C_{T_{\text{val}} > 750 \text{ K}}) < 10$ for the fit.

The resulting distribution of $\log_{10}(C_{T_{\text{val}} < 750 \text{ K}} / C_{T_{\text{val}} > 750 \text{ K}})$ is shown in Fig. B.1. The distribution in Fig. B.1 enables us to calculate a σ value as shown in the Figure. This value is then used to constrain the range over which the rate constants are varied in the Monte Carlo results shown in Fig. 8. The rate coefficients can be over- or underestimated when using rate coefficients that are not valid for temperatures below 750 K. The results suggest

that it is more likely that the reaction rate would be underestimated when using $C_{T_{\text{val}} > 750 \text{ K}}$ (estimated coefficients) instead of $C_{T_{\text{val}} < 750 \text{ K}}$ (measured coefficients). However, due to the low number of statistics and the fact that both over- and underestimation of the coefficients is possible, we considered only the standard deviation, σ , to compute the log-normal distribution for the MC runs and assumed $\mu=0$.

To compute the σ value for the type 3 reactions, we used the same procedure as for the type 2 reactions. Homologous nitrogen species reaction kinetics for unknown phosphorus species rate coefficients were compared in Bains et al. (2021). They showed that some rate coefficients of the analogue phosphorus and nitrogen reactions (C_P and C_N , respectively) agreed within about one order of magnitude. However, most of the phosphorus-containing reactions shown are only valid at a temperature above 1000 K. For the analogue reactions of PH_3 and NH_3 , the difference between the rate coefficients is several orders of magnitude. We estimated the uncertainty when using this approach with 24 reactions, for which we found the corresponding C_P and C_N in the NIST (R1, R3, R5, R6, R8, R11, R12, R13, R14, R16, R18, R21, R22, R23, R24, R25, R26, R27, R28, R29, R31, R50, R51, and R53 in Table A.1).

Figure B.2 suggests that it is more likely that the reaction rate would be underestimated when using C_N (estimated coefficient) instead of C_P . However, both an over- and underestimation of the coefficients is possible. We only considered σ to compute the log-normal distribution for the MC runs and assumed μ to be zero.

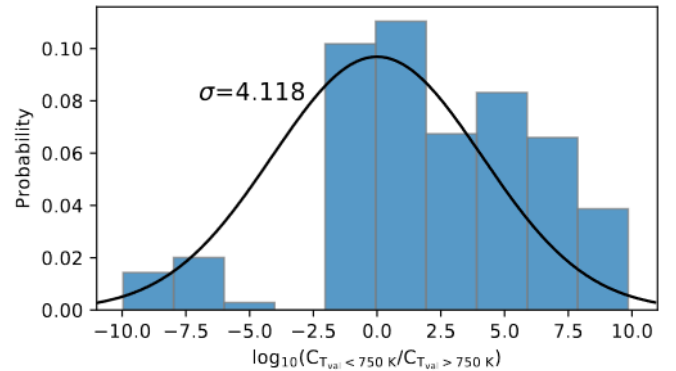


Fig. B.1. Histogram showing the ratio of measured to estimated rate coefficients of type 2 reactions ($C_{T_{\text{val}} < 750 \text{ K}} / C_{T_{\text{val}} > 750 \text{ K}}$) in blue. The fit of the data to a log-normal distribution with $\sigma=4.118$ and $\mu=0$ is shown in black.

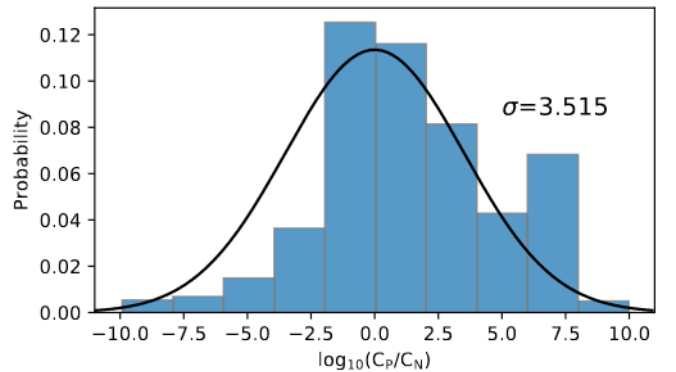


Fig. B.2. Histogram showing the ratio of measured to estimated rate coefficients of type 3 reactions (C_P / C_N) in blue. The fit of the data to a log-normal distribution with $\sigma=3.515$ and $\mu=0$ is shown in black.